Search for Causes of the Low Epithermal Neutron Flux Anomaly in the Arabia Terra Region (Mars)

A. T. Basilevsky[a], A. V. Rodin[b], J. Raitala[c], G. Neukum[d], S. Werner[d], A. S. Kozyrev[b], A. B. Sanin[b], I. G. Mitrofanov[b], J. W. Head[e], W. Boynton[f], and R. S. Saunders[j]

[a] Vernadsky Institute of Geochemistry and Analytical Chemistry, Russian Academy of Sciences, ul. Kosygina 19, Moscow, 119991 Russia

[b] Space Research Institute, Russian Academy of Sciences, ul. Profsoyuznaya 84/32, Moscow, 117997 Russia

[c] Astronomy Department, University of Oulu, Finland

[d] Institute of Geosciences, Free University, Malteserstr. 74-100, D-12045 Berlin, Germany

[e] Department of Geological Sciences, Brown University, Providence, RI 02912, USA

[f] Lunar and Planetary Laboratory, University of Arizona, Tucson, AZ 85721, USA

[j] Jet Propulsion Laboratory, Pasadena, CA 91109, USA

Received December 9, 2005

Abstract—A geologic analysis of 274 images acquired by the high-resolution MOC camera onboard the *Mars Global Surveyor* spacecraft within the Arabia Terra low neutron flux anomaly (which is indicative of an anomalously high abundance of hydrogen: up to 16 wt % of the equivalent amount of water) was performed. Correlation between the enhanced abundance of equivalent water with the presence of dust on the surface was found. Since dust plays a key role in condensation of water from the atmosphere, we suppose that the anomalies could result from the retention of atmospheric moisture. To analyze this suggestion, we performed a theoretical modeling that allowed us to map the planetary-scale distributions of several meteorological parameters responsible for the atmospheric moisture condensation. Two antipodal regions coinciding rather well with the Arabia Terra anomaly and the geographically antipodal anomaly southwest of Olympus Mons were found in the maps. This suggests that the anomalies are rather recent than ancient formations. They were probably formed by a sink of moisture from the atmosphere in the areas where present meteorological conditions support this sink. Geological parameters, primarily the presence of dust, only promote this process. We cannot exclude the possibility that the Martian cryosphere, rather than the atmosphere, supplied the studied anomalies with moisture during their formation: the thermodynamic conditions in the anomaly areas could block the moisture flux from the Martian interior in the upper regolith layer. The moisture coming from the atmosphere or from the interior is likely held as chemically bound water entering into the structure of water-bearing minerals (probably, hydrated magnesium sulfates) directly from the vapor; or the moisture precipitates as frost, penetrates into microfissures, and then is bound in minerals. Probably, another geologic factor—the magnesium sulfate abundance—works in the Arabia Terra anomaly.

PACS numbers: 96.30.Gc

DOI: 10.1134/S0038094606050017

INTRODUCTION

This study continues attempts to understand the nature of the anomalously low epithermal neutron flux from the Martian surface in the regions of Arabia Terra and southwest of Olympus Mons (Fig. 1). These anomalies were found from analyzing the Neutron Spectrometer (NS) and High-Energy Neutron Detector (HEND) measurements onboard the *Mars Odyssey* spacecraft (Boynton et al., 2002; Feldman et al., 2002; Mitrofanov et al., 2002, 2003). They reside at low latitudes (20°S–40°N), where, as a rule, the neutron flux is substantially higher. The enhanced and low neutron fluxes are indicative of respectively decreased and increased abundances of hydrogen in the surface layer material.

Hydrogen in this layer is evidently in the form of water: free (water ice) or physically (absorption) or chemically (as OH and H_2O in mineral structures) bound. Assuming the water content in the surface layer at the landing site of *Viking 1* to be approximately 1 mass % (summarizing the data by Biemann et al. (1977)), Boynton et al. (2002) used the NS measurements and made a preliminary estimate of the water abundance of ~3.5–4% in the surface rocks of the two anomalous regions mentioned above. More recently, Feldman et al. (2005) estimated the water abundance in the surface rocks in the southwestern part of the Arabia Terra anomaly, where gray crystalline hematite is accumulated (Christensen et al., 2001b) and where the *Opportunity* rover landed (Squyres et al., 2004a, 2004b), to be 6.5 ± 1.0 mass %. Mitrofanov et al. (2004)
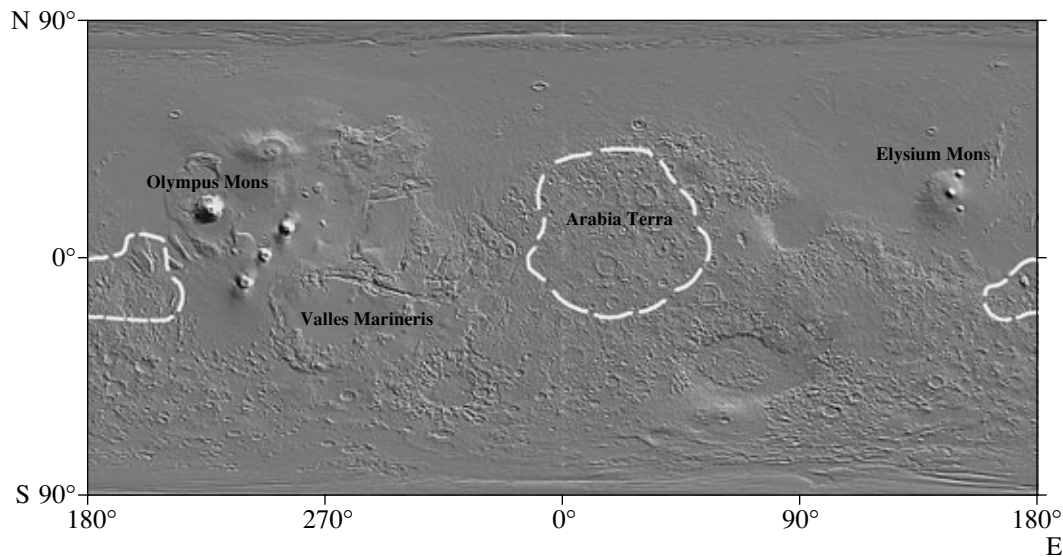
Fig. 1. Martian surface relief map built from MOLA laser altimetry. White contours show the boundaries of the regions with anomalously low epithermal neutron fluxes: Arabia Terra (in the center) and its antipodal area southwest of Olympus Mons (on the left and on the right).

considered a two-layer model of the anomalies in Arabia Terra and the southwest of Olympus Mons: the upper "dry" layer of 26–32 g/cm^3 in mass (~15–20 cm) contains 2 mass % of water, while the water-enriched layer is under it. Within the framework of this model, the mean water abundance is 9% in the lower layer of the Arabia Terra anomaly and reaches 16% in the "wettest" area of this anomaly (10° N, 30° E).

The anomalies under consideration are at latitudes where it is on average rather warm and, according to calculations of Farmer and Doms (1979) and Mellon and Jakosky (1993, 1995), water ice should be unstable at a depth where the epithermal neutron flux is generated (down to 1–2 m). From this, Basilevsky et al. (2003) inferred that the decrease in the neutron flux observed in these regions is induced by the enhanced abundance of chemically bound water, e.g., water in the form of clays, hydroxides, and hydrosalts. Since such model calculations always simulate the real situation only approximately, it is worth supporting or disproving the conclusion on the absence of ice at this depth by observational data. For example, the presence of small "permafrost" forms, such as polygons or solifluction terraces, could doubt the correctness of the model calculations, which forbid the presence of ice in the upper part of the surface layer. A search for such forms requires the analysis of images with a resolution better than several meters per pixel.

In any case, it would be interesting to consider whether there is any peculiarity in the geologic structure of the anomalies in Arabia Terra and southwest of Olympus Mons. It turned out that a specific character of these areas had been already discussed in the literature. Schultz and Lutz (1988) pointed out that there are

deposits in these areas which may be an analogue of the layered deposits currently observed in the polar regions of Mars. Taking into account the antipodal character of the mentioned areas, these authors suggested that they are the relics of deposits of the ancient Martian polar caps. When the high-resolution MOC images were obtained, similar deposits were found in some other regions of Mars (see, e.g., Malin and Edgett, 2000), which weakens the idea on their uniqueness and, therefore, the position of the hypothesis on the ancient polar caps. In the paper by Newsom et al. (2003) describing the Arabia Terra southern region, which partly coincides with the southwestern part of the Arabia Terra anomaly, the layered deposits are considered to be lacustrine sediments.

Basilevsky et al. (2003) failed to find links between the epithermal neutron flux and the character of geologic structure of the areas presented in the synoptic geologic maps of Mars (Greeley and Guest, 1987; Scott and Carr, 1978; Scott and Tanaka, 1986). In the authors' opinion, the lack of this correlation stems from the fact that these maps show the distribution of fairly thick (tens and hundreds of meters or even kilometers) geological bodies (lavas, impact breccias, and sediments); and the 1- to 2-m layer, where the epithermal neutron flux originates from, is simply not visible for a morphological analysis, on which these maps are based, and has no influence on the identification of geologic units. For geological analysis of this thin blanket, Basilevsky et al. (2003) suggested to examine high-resolution (meters) images (see, e.g., Malin and Edgett, 2000; Malin et al., 2001). The first part of the present paper is a realization of this suggestion.
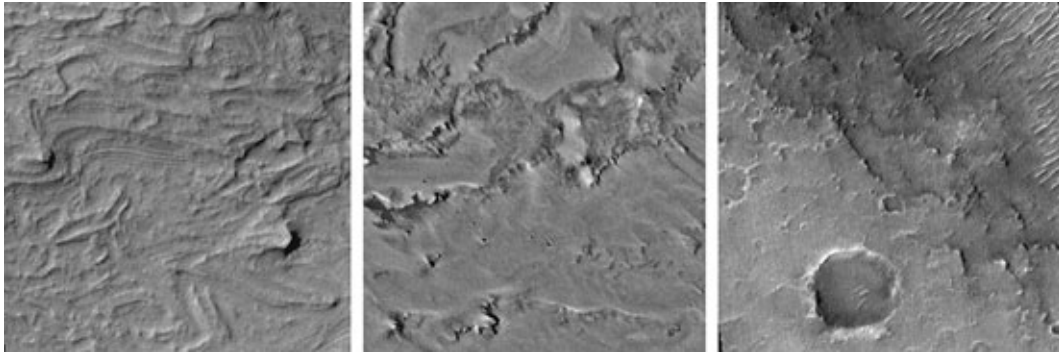
Fig. 2. Layered deposits at observational stations 46 (a bottom of a 70-km crater, 1.35° N, 31.09° E), 96 (a bottom of another 70-km crater, 3.52° N, 57.08° E), and 148 (the intercrater plain, 18.07° S, 65.09° E). The fragments of the MOC M18-01484, M11-03418, and M08-00816 images. The image resolution is 3 m per pixel. The area covered by each fragment is 900×900 m.

GEOTRAVERSE ACROSS THE ARABIA TERRA ANOMALY

Since the Arabia Terra epithermal neutron flux anomaly occupies a large area, the number of high-resolution images within this region is rather high. Therefore, we selected for our analysis the MOC images along a geotraverse. A geotraverse is a strip about 10 areographic degrees wide, which starts at 47° N, at the north of the northern boundary of the anomaly, in the contact zone between the Northern Plains and the cratered highland of Arabia Terra. Further this strip goes southward along the 25° E meridian across the cratered highland terrain approximately to the center of the anomaly. Then the geotraverse goes eastward along the 5° N parallel (in order to keep out of possible latitude climatic effects, at least in this part of the geotraverse). At 55° E the geotraverse crosses the anomaly boundary and goes to 70° E, where the volcanic plains of Syrtis Major Planitia (the Nili Patera region) are developed; turns to the south; arrives again in the cratered highland at 1°–5° S; and terminates at 20° S. We examined all 152 narrow-angle MOC images available for this zig-zag strip (up to the moment when this part of the study was carried out, that is, by December 2002). Their resolution ranges from 1.5 to 12 m per pixel. We also used the context MOC images with a 240-m resolution within this region. Thus, the geotraverse contains 152 observational stations. The image resolution is 1.5, 2.4, 3, 4.5, 6, and 12 m for 18, 1, 87, 24, 21, and 1 stations, respectively. While examining the images, we paid attention to the presence of layered deposits, fluvial valleys, polygons, debris flows, dunes, dust devil traces, and to the type of prevailing surface texture. The minimal thickness of the loose surface mantle in a given place was estimated from the morphology of small impact craters. The results of this analysis are given below.

Layered Deposits

The typical examples of the layered deposits and the stations where they were observed are shown in Figs. 2 and 3, respectively. Layered deposits are seen as erosion terraces with scarps in the craters and intercrater areas, quite often in closed basins. Evidently, they are seen in the places where they are eroded and partly destroyed by wind. This suggests that the constituting material can be blown out and, therefore, it is rather loose and fine-grained. The layers are roughly horizontal. Since the vertical projection of the width of scarps observed in the images is 10–20 m for most layers, the typical layer thickness is less than several meters. The elevation of the surface where layered deposits are observed varies from –1 to +3 km above the mean level of the Martian surface.

From the set of characteristics listed above, the layered deposits of Arabia Terra can be considered as the dust deposited from the atmosphere (this category also includes the dust component of the layered polar deposits), fine-grained volcanoclastic sedimentations, or sediments deposited in the aquatic environment. From
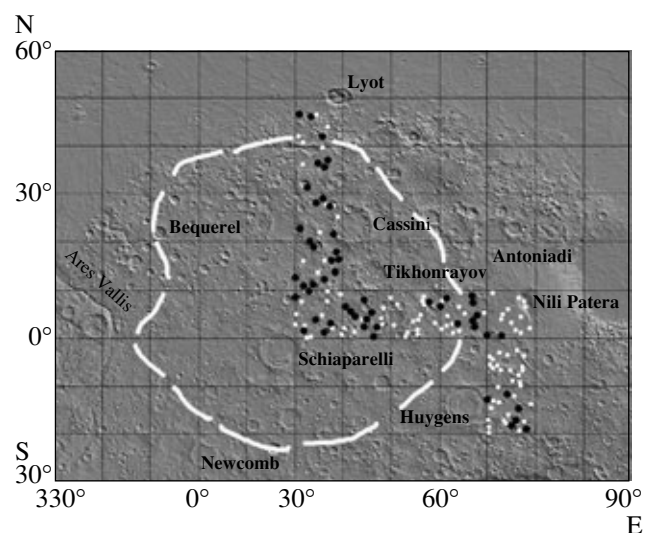
Fig. 3. Presence (black dots) and absence (white dots) of outcrops of layered deposits within the geotraverse.
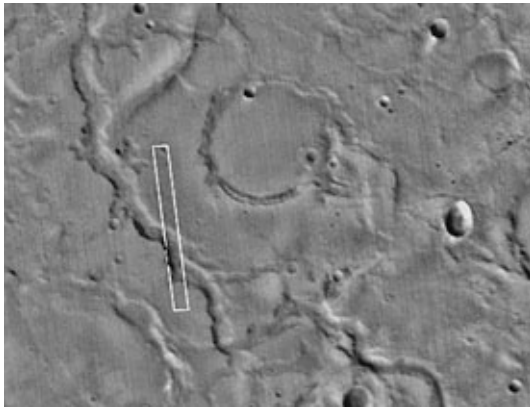
Fig. 4. Ancient fluvial valley in the region of observational station 55 (6.55° N, 26.51° E). The wide-angle MOC image M10-020020. The area covered by the image is 120 × 120 km.

Fig. 5. Fluvial valleys present (black dots) and absent (white dots) within the geotraverse.

the analysis by Newsom et al. (2003), who paid attention to the link between the layered deposits of the southern part of Arabia Terra and the valley system and topographic barriers, it follows that at least a part of them are lacustrine sediments. Apparently, this inference can be extended to most of layered deposits within the geotraverse. According to Newsom et al. (2003), the hematite deposit is a fraction of the layered deposits of this area, which is confirmed by observations from the *Opportunity* rover (see below). The age of these sediments, as follows from the crater count (Lane et al., 2003), exceeds 3.8 Gyr, i.e., the Early Noachian, while the time of their aeolian deflationary exhumation is only several million years.

Layered deposits were found at 54 from 152 observational stations. Almost all of them are within the cratered highland. Layered deposits show no evident preference to be inside or outside the anomaly (see Fig. 3).

Fluvial Valleys

An example of a fluvial valley typical of the examined area is presented in Fig. 4, while the corresponding observational stations are shown in Fig. 5. The valleys are tens to several hundred kilometers long, while their width ranges from 1 to 5 km. They are meandering and have tributaries. The latter suggests that they were probably formed by the water of atmospheric precipitation (see, e.g., Carr, 1996; Howard et al., 2005; Irwin et al., 2005). The analysis by Newsom et al. (2003) shows that the location of valleys and the direction of flows were extensively controlled by the topography of ancient impact craters and basins. Newsom et al. point out to the link between the fluvial valleys and the Early Noachian layered deposits, which means that the valleys here are mainly very old. However, the authors also described the case of a small younger valley in this study. Like in the case of layered deposits, the elevation of the surface where the fluvial valleys are observed
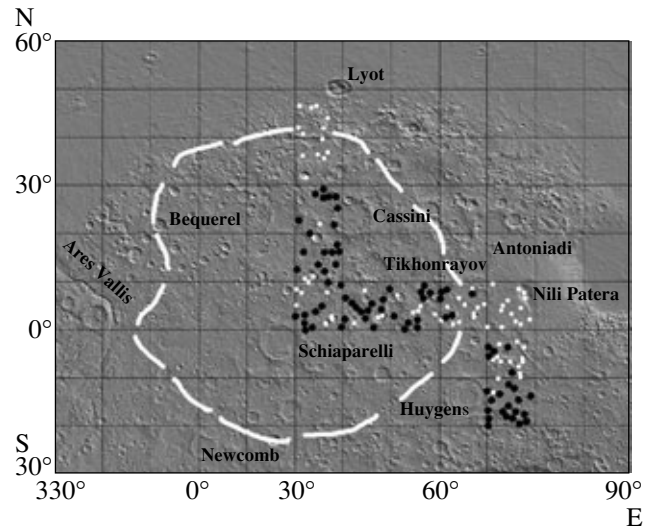
varies from –1 to +3 km above the mean level of the Martian surface.

Fluvial valleys were found at 79 of 152 observational stations. They are almost always observed within the cratered highland. Fluvial valleys show no evident preference to be inside or outside the anomaly (see Fig. 5).
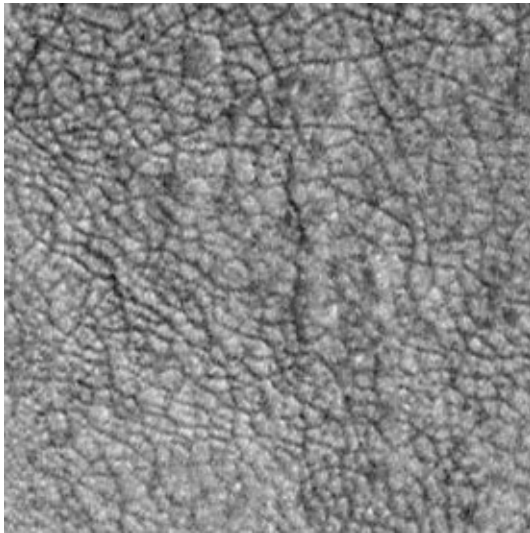
Polygons

There are only few (four) stations within the geotraverse where polygons are observed. These are stations 1, 3, 4, and 7, all at the northern end of the geotraverse. Figure 6 shows the area of station 4, which is covered by the image with a 1.5-m resolution. Figure 7 shows the location of the stations with polygons. The diameter of polygons displayed in Fig. 6 varies between 7 and 40 m. In most cases, it ranges from 10 to 15 m.
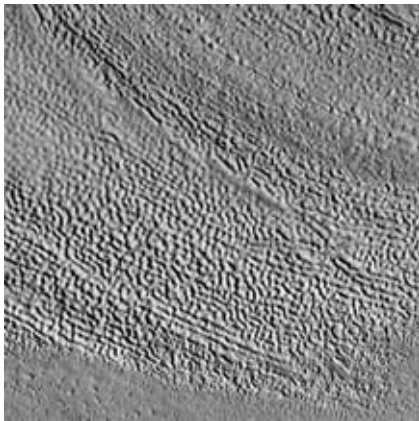
Debris Flows

There are also very few (only seven) stations within the geotraverse where debris flows are observed. These are stations 6, 8, 10, 12, and 16. All of them are also in the northern part of the geotraverse, but do not coincide with the places from where polygons can be observed. Figure 8 shows the area of station 10, which is covered by the image with a resolution of 3 m. The locations of the stations with debris flows are displayed in Fig. 9.

Dune Fields

Examples of dune fields are presented in Fig. 10, and Fig. 11 shows where these fields were observed in sufficient quantity within the geotraverse. Most of the dune fields consist of linear dunes 10–20 m wide and
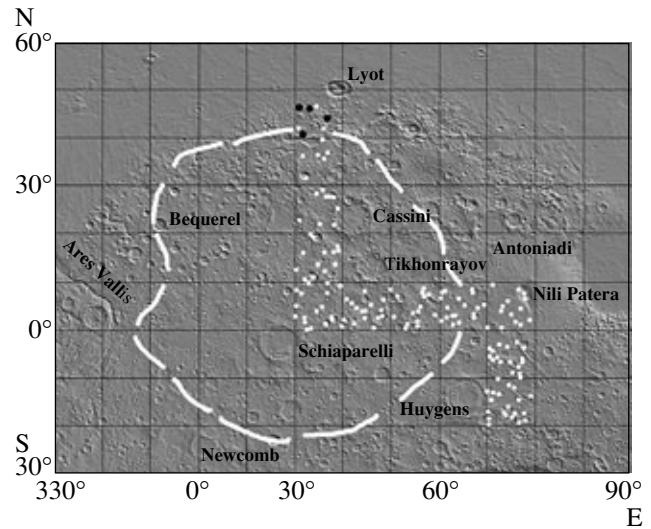
Fig. 6. Polygonal relief forms at station 4 (44.41° N, 26.69° E). The fragments of the MOC M03-00046 image with a resolution of 1.5 m per pixel. The area covered by the fragment is 450 × 450 m.

Fig. 7. Polygons present (black dots) and absent (white dots) within the geotraverse.
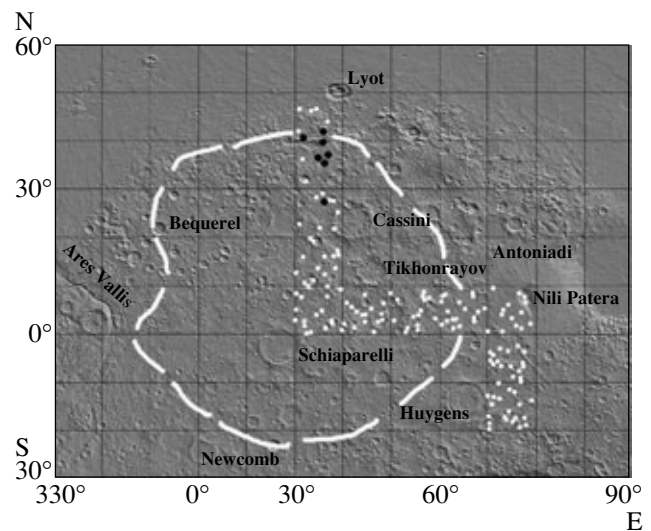

Fig. 8. Debris flow fragment at station 10 (36.87° N, 24.65° E). The fragment of the MOC M03-01119 image with a resolution of 3 m per pixel. The area covered by the fragment is 900 × 900 m.

Fig. 9. Debris flows present (black dots) and absent (white dots) within the geotraverse.

100–300 m long; the distance between the crests of the neighboring dunes is about 20–30 m (Fig. 10, left). There are almost no dune fields in the northern part of the geotraverse. A dune field was observed there only within the area of station 6 in the crater with a diameter of about 2.5 km. The dune fields were found at 9 stations inside the latitude segment of the geotraverse: at 6 stations within the anomaly, at 2 stations on its eastern boundary, and at 1 station further to the east of the anomaly in the Nili Patera region. In the latter case (Fig. 10, right), the barchan fields and single barchans are observed. For the barchans of typical planimetrically crescent shape, the steep windward and gentle lee-

ward slopes are 10–20 and 100–150 m in width, respectively. The distance between acute ends of typical barchans is 150–200 m. The barchans sometimes join end-to-end to form sinuous linear structures about 1 km long. The maximal concentration of dune fields is observed in the southern part of the geotraverse to the east of the Huygens Crater about 600 km from the anomaly boundary (Fig. 11). The dune fields here resemble those shown in Fig. 10 (left). In general, one can say that the dune formations are present both within the anomaly and beyond its boundaries and show neither positive nor negative clear correlation with the anomaly.
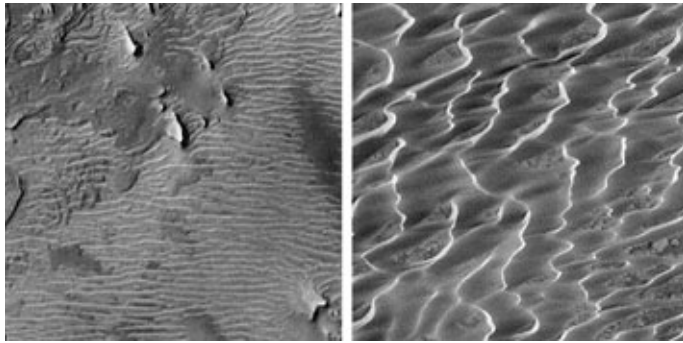
Fig. 10. Dune fields at stations 49 (left) and 114 (right) (1.35° N, 26.51° E and 6.94° N, 67.92° E, respectively). The fragments of the MOC M18-01484 and M04-01239 images with a 3-m resolution per pixel. The area covered by each fragment is 900 × 900 m.
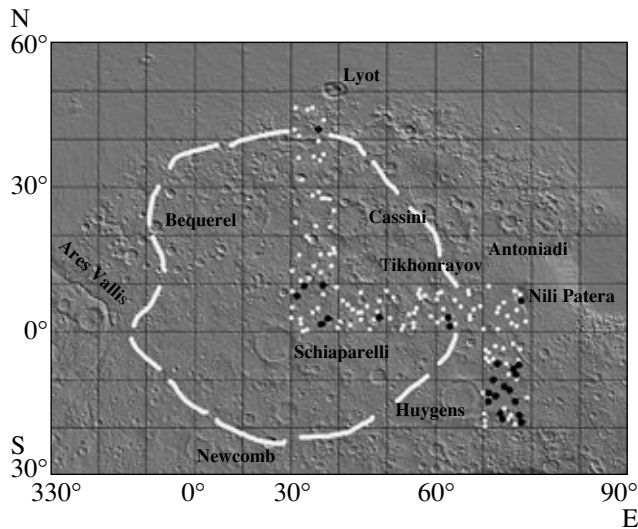
Fig. 11. Dune fields present (black dots) and absent (white dots) within the geotraverse.
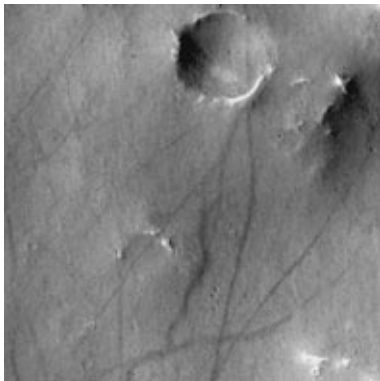
**Fig. 12.** Dust devil traces at station 45 (2.88° N, 21.84° E). The fragment of the MOC M02-01515 image with a resolution of 2.4 m per pixel. The area covered by the fragment is 700 × 700 m.

Dust Devil Traces

An example of dust devil traces is presented in Fig. 12, and Fig. 13 shows where dust devil traces were observed in sufficient quantities within the geotraverse. Traces are variously dark, rectilinear, arched, and sometimes sinuous strips with fuzzy boundaries. They are from several hundred meters to 1.5–2 km long, while their width ranges from the limit resolution of the image to 20–30 m. Sometimes these traces intersect craters several hundred meters in diameter preserving their direction and the intensity degree. They are seen at 19 stations always within the anomaly in the latitudinal segment of the geotraverse. Dune fields are also developed in this area; however, either dust devil traces or dune fields are usually observed at a certain station. Both formations are seen together only in one case (station 57). However, there are quite a lot of dust devil traces at this station, whereas the dune fields here are isolated and small. This example confirms rather than refutes the antagonism of dust devil traces and dune fields.
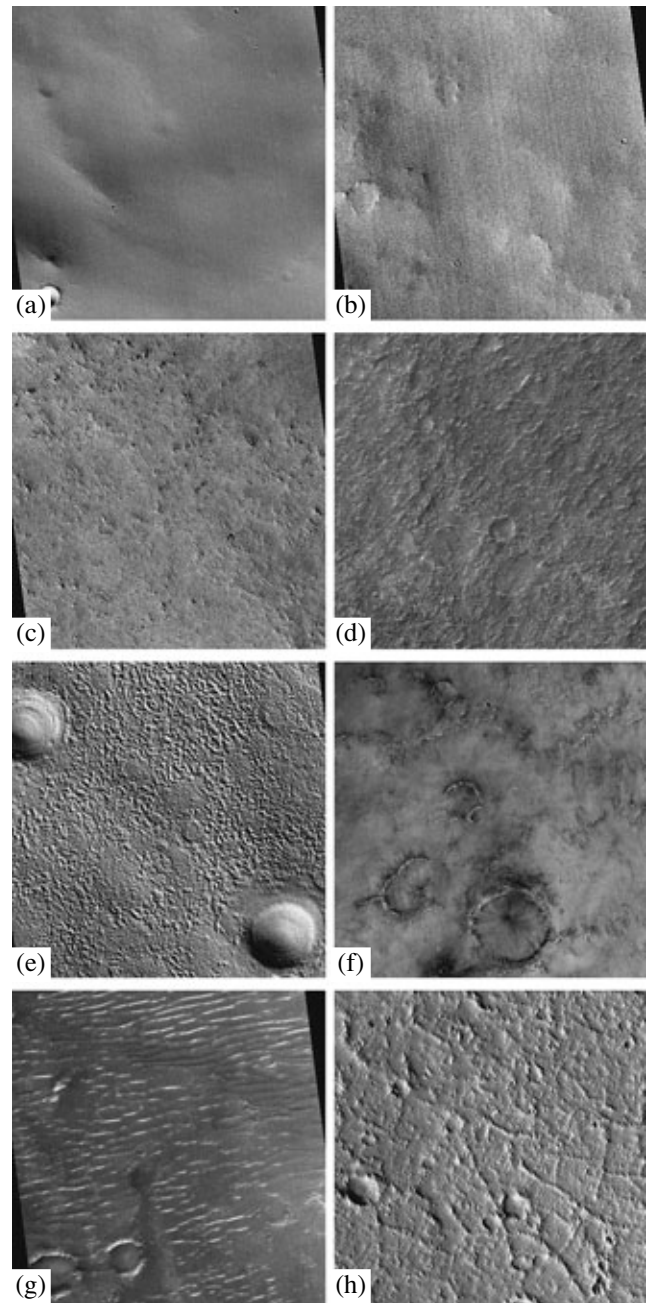
Surface Texture

Seven main surface types can be distinguished within the geotraverse, namely, smooth, fine-texturized, knobby, ridged, pitted, mottled, and duned ones (Fig. 14). The surface was called *smooth* if no or almost no complicating elements are seen there (Fig. 14a). Such a surface is probably typical of the aeolian blankets of fine-grained material. The surface was called *fine-texturized* when some complicating features were seen there but their nature was unclear because of insufficient resolution (Fig. 14b). It is obvious that the relation between the smooth and fine-texturized types depends on the image resolution. The nature of fine features making the surface fine-texturized is obscure. Most likely, this is aeolian ripples, small deflation depressions, or camera noise (M.A. Kreslavsky, private communication). The *knobby* surface is characterized by the presence of many planimetrically isometric knobs several tens of meters across. These knobs are probably spots where the material is more resistant to deflation (Fig. 14c). The *ridged* surface is characterized by the presence of ridges tens to several hundreds of meters long (Fig. 14d). Sometimes they are evidently remnant landforms. Sometimes it can be suspected that the ridges are aeolian ripples. The *pitted* surface contains a lot of planimetrically isometric pits typically tens meters across (Fig. 14e). They can be deflation depressions or thermokarst landforms, as well as impact craters destroyed to a variable degree. The surface was called *mottled* if its appearance was determined by diffuse bright patches of probably aeolian nature (Fig. 14f). And, finally, the surface was called *duned* when clearly seen dunes and barchans dominated there (Fig. 14g). Sometimes the surface contains the features of different texture types. For example, the
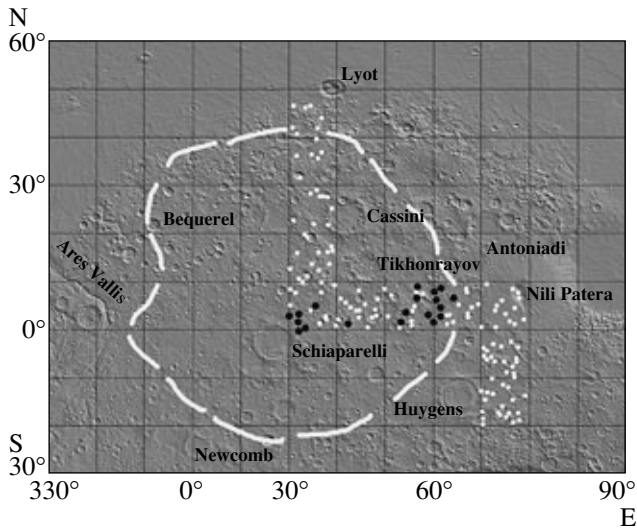
Fig. 13. Dust devil traces present (black dots) and absent (white dots) within the geotraverse.

surface, which can be called ridged–knobby, is shown in Fig. 14h.

Figure 15 shows the surface textures observed at 87 stations described by 3-m resolution images and at 1 station described by a 2.4-m resolution image. Quite often, different texture types are seen within an image. For example, the areas of smooth, duned, and knobby surfaces are seen in the image showing station 95. In such cases, the surface type dominating by area was shown. The smooth surface was accepted as dominant at 36 stations located both inside and outside the anomaly. The fine-texturized surface dominated at 15 stations; all of them were within the anomaly. The relation between the smooth and fine-texturized surfaces changes in favor of the second one, when the image resolution improves. For example, the fine-texturized surface is seen in 17 from 18 images of a 1.5-m resolution, and only one image shows the smooth surface. When the 3-m resolution images were examined, the knobby surface dominated only at one station within the anomaly, but was observed as a secondary type in some other places including the areas beyond the anomaly boundaries. The ridged surface dominated at 16 stations, and only one of them was within the anomaly, while the other 15 were to the southeast of the anomaly in the area with dune relief in the vicinity of the Huygens Crater. The pitted surface is typical of 3 out of 88 stations; one of them is inside the anomaly, and the other 2 are outside. The mottled surface is typical of the eastern boundary of the anomaly and further eastward. The dune texture was also observed at the eastern boundary of the anomaly and further to the east and southeast. In general, the predominance of smooth and, particularly, fine-texturized surfaces can be noted within the anomaly. However, the latter is probably connected with the predominance of the 1.5-m resolution images there.

Fig. 14. Main types of the surface texture within the geotraverse: (a) smooth (station 30; 14.17° N, 26.51° E), (b) fine-texturized (station 70; 2.88° N, 40.93° E), (c) knobby (station 95; 5.86° N, 55.57° E), (d) ridged (station 136; 12.79° N, 60.03° E), (e) pitted (station 15; 28.58° N, 24.38° E), (f) mottled (station 100; 4.70° N, 58.10° E), (g) duned (station 143; 17.04° S, 67.76° E), (h) ridge–knobby (station 27; 16.54° N, 21.33° E). All the examples are the fragments of the 3-m resolution images covering the area 1.5×1.5 km.

Minimal Thickness
of the Loose Surface Mantle

The minimal thickness of the blanket of loose deposits was determined depending on whether rims of small impact craters are seen from under this blanket or
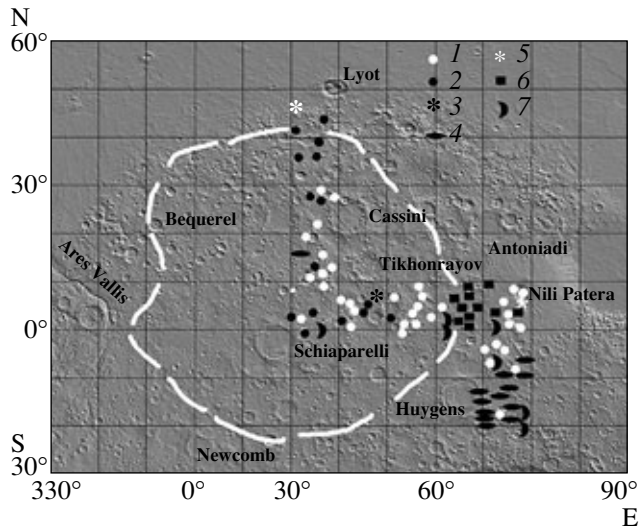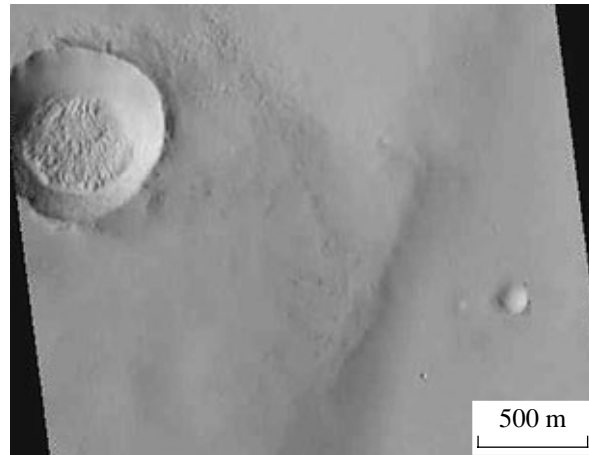
Fig. 15. Distribution of the main types of surface texture within the geotraverse.

Fig. 16. Example demonstrating how the thickness of the blanket of loose deposits is found from the size of craters whose rims are hidden or not hidden with this blanket (28.33° N, 26.40° E). At the upper left, there is a crater 800 m across with a circular rim projecting above the surrounding terrain. At the bottom right, there is a crater 150 m across whose rim is completely covered with a blanket of loose deposits. The fragment of the MOC M20-00789 image with a resolution of 6 m per pixel.

the crater is seen as a rimless depression (Fig. 16). This method was used by Edgett et al. (1997) for estimating the thickness of the blanket of loose deposits in the so-called "Stealth" region in southwestern Tharsis Mons. If the crater is seen as a rimless depression, the thickness of the blanket hiding the rim can be estimated from the known dependence of the rim height h above the surrounding surface on the crater diameter D ($h \approx 0.035D$; Basilevsky et al., 1983; Pike and Davis, 1984). Since the craters can be completely covered with such a blanket and we simply cannot see them, the estimate from the calculated rim height of the distinguished craters is minimal. We determined the average value of this quantity for 11 geotraverse areas with approximately the same number of observational stations within which such an estimate could be obtained (Fig. 17). As seen in the figure, the average minimal thickness of the blanket within the geotraverse ranges from 5.2 to 15.4 m with no noticeable connection to the fact whether a specified area belongs to the anomaly or not.

### Discussion of the Geotraverse Analysis

It follows from all of the above that the presence of layered deposits, fluvial valleys, polygons, debris flows, and dunes and the thickness of the blanket of loose deposits show no connection with whether the area under consideration is within the anomaly or not. The connection was found only for dust devil traces: they were observed only within the anomaly boundaries, although not throughout the entire geotraverse. Probably, there is also a link with the type of the dominating surface texture: the smooth and fine-texturized surfaces dominate inside the anomaly.

We expected to find a link between the enhanced water abundance in the surface layer and the presence

of layered, probably lacustrine (Newsom et al., 2003; Squyres et al., 2004a; 2004b), sediments and fluvial valleys. These features were formed with the participation of liquid water, and it is natural to suppose that their material may contain a crystallization water. However, our analysis has shown that there is no direct correlation between the water abundance in the surface layer and the presence of these structures. Probably, the point is that the portion of the area occupied by these structures is small, and their contribution to the signal measured with neutron spectrometers is not large.
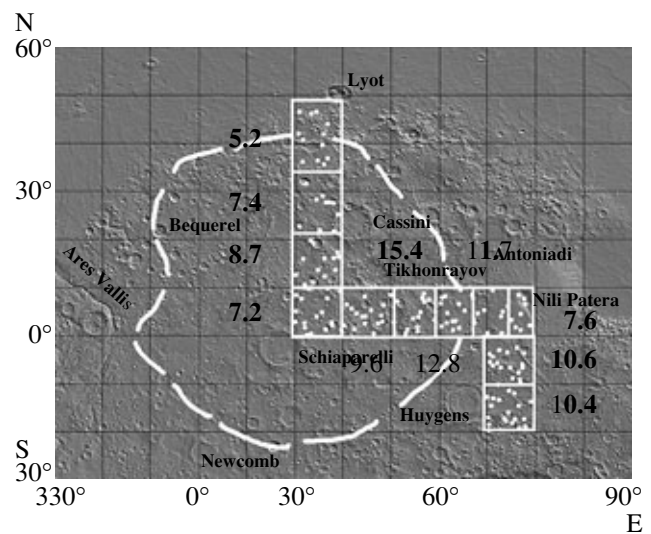
Fig. 17. Distribution of the mean thickness of the loose surface mantle within the geotraverse.

Polygons and debris flows were observed only in the northernmost part of the geotraverse, and it is evident that they have no connection to the anomaly of water distribution in the surface layer studied here. The fact that dunes are found both inside and outside the anomaly shows that the material composing them is not necessarily characterized by increased water abundance. Since the dunes are known to be formed from the material of sand dimensions, the aforementioned antagonism between the presence of dune fields and dust devil traces is clear. Dust devil traces require a considerable temperature contrast between the surface and the near-surface atmospheric layer (Renno et al., 2000; Ferri et al., 2003). Such conditions are usually realized in places with a low thermal inertia of the surface (Jakosky et al., 2000), that is, in the places where there is dust and no sand on the surface. Consequently, the above-mentioned link between the enhanced water abundance and the dust devil traces indicates that the increase in water abundance is somehow connected with the presence of dust on the surface.

The predominance of smooth and, particularly, fine-texturized surfaces within the anomaly also points to a probable link with the dust presence. However, as has been noted above, the observational effect (the image resolution) cannot be excluded. The lack of correlation between the enhanced water abundance and the thickness of the blanket of loose deposits probably means that the key point is not the thickness of deposits, but the thickness-independent properties of the upper 1–2 m of this blanket.

The overall result of the geotraverse analysis is the following: the increased water abundance inside the Arabia Terra anomaly is probably somehow connected with the presence of dust on the surface, but the nature of this link remains obscure.

PERSISTENTLY WET AND PERSISTENTLY DRY SPOTS WITHIN ARABIA TERRA: GEOLOGICAL ANALYSIS

Some uncertainty in the results on the geotraverse can be connected, at least in part, with the nonuniformity of the water-abundance distribution within the Arabia Terra anomaly. With an average value of 9%, the water abundance is noticeably higher (up to 16%) in some areas, while in the others it goes down to non-anomalous 2% (Mitrofanov et al., 2004). Consequently, it seems important to perform a more detailed spatial analysis of the water distribution within the anomaly. To that end, we compare the geologic structure of the wettest and driest spots. Since the HEND data (as well as the data from other instruments) contain stochastic noise, which can result in false minimums and maximums, we used a map of a so-called sigma parameter (Kozyrev et al., 2003). This parameter shows the statistics of time variations of the epithermal neutron flux measured for each map pixel. The value of sigma was calculated as a ratio of the difference between the read-
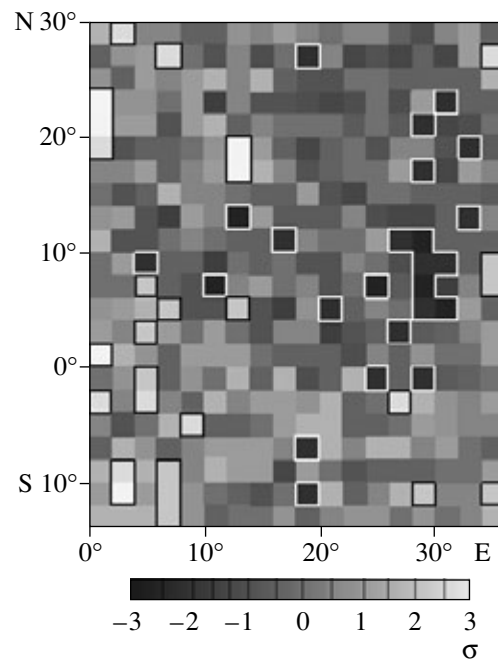

Fig. 18. The sigma parameter map for a part of the Terra Arabia anomaly. White and black lines outline the persistently wet and persistently dry spots, respectively.

ing in a given pixel and the readings averaged over the entire Arabia Terra region to the reading error in the given pixel. If the sigma parameter is known, not only the areas of a neutron-flux depression can be distinguished, but the significance of this depression can also be characterized, because the sigma parameter also depends on the statistical error of the measurement. Thus, "persistently wet" and "persistently dry" spots were revealed against the background of areas with unsteady neutron fluxes. During the whole period of observations, these spots are characterized by the persistently low or persistently high flux, respectively. Such a map with pixels of 2×2 areographic degrees was built by Kozyrev et al. (2003). One of its versions is used in the present analysis (Fig. 18).

This map covers the region from 14° S to 30° N and from 324° W to 360° W, which is about half of the anomaly area. In this region, we selected 18 persistently wet and 19 persistently dry spots. Single pixels or their clusters were considered as a persistently wet spot if the sigma parameter there was less than –2; and they were considered as a persistently dry spot, if the sigma parameter there was larger than +2. We examined all 122 narrow-angle MOC images covering these 37 spots: 47 and 75 images for wet and dry spots, respectively. The image resolution ranges from 1.5 to 12 m. To eliminate the possible influence of the image resolution on the analysis results, we first examined the images with a resolution of 3 m. From these 38 images, 16 and 22 images are for wet and dry spots, respectively. Examining these 38 images, we found that the
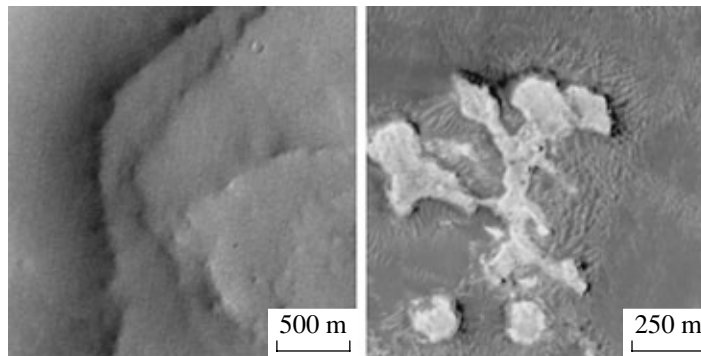
Fig. 19. Two types of layered deposits in the region under consideration. Left: type 1, the relatively bright outcrops of layered deposits against the background of approximately the same brightness (11.67° N, 22.88° E); right: type 2, the bright outcrops of layered deposits against the dark background (16.80° N, 30.28° E). The fragments of the MOC E05-03422 and SP2-39103 images with a resolution of 6 and 3 m, respectively.
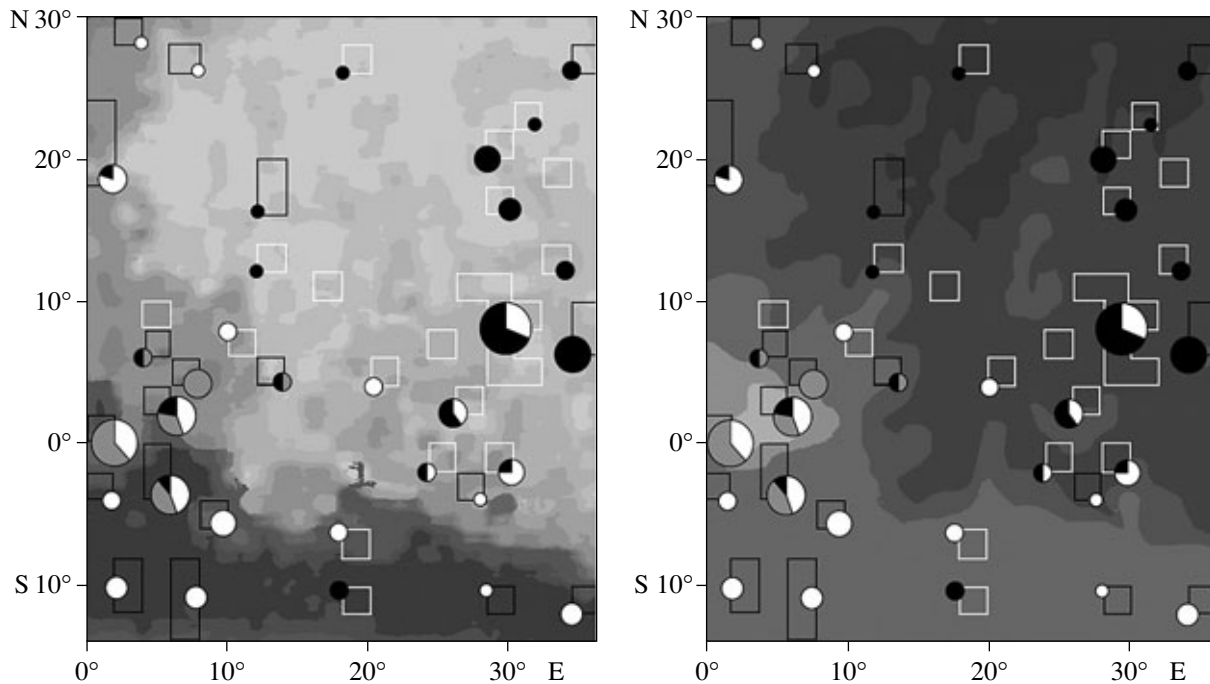
Fig. 20. Maps of albedo (left) and thermal inertia (right) in the region under consideration. The persistently wet and persistently dry spots are outlined. The circles with black, grey, and white sectors show the number of MOC images covering a certain area and the portion of images where layered deposits are seen or not seen (see the text).

layered deposits observed on the surface dominate, to some extent, within the wet spots.

However, a more careful analysis revealed that the outcrops of layered deposits are rather vast and can be well distinguished even in the 12-m resolution images. Therefore, we resumed the examination of all 122 images. As a result, the previously suggested link between the layered deposits and persistently wet spots has faded, but, simultaneously, another correlation has emerged. We distinguished two types of layered depos-

its: (1) relatively bright outcrops of layered deposits against the surrounding geologic landforms of almost the same brightness and (2) relatively bright outcrops of layered deposits against a relatively dark background (Fig. 19). It was found that the layered deposits of the first type dominate inside persistently wet spots, while the second type of deposits is mostly found inside persistently dry spots.

In attempting to explain this fact, we used the albedo and thermal inertia maps built for this territory based on

the data of the infrared (IR) spectrometer TES (the *Mars Global Surveyor* mission) (Christensen et al., 2001a; Mellon et al., 2000). Figure 20 (left) presents the albedo map of the studied territory; the areas of high (up to 0.3) and low (0.13–0.15) albedo are shown in light and dark colors, respectively. The thermal inertia map is in the figure on the right; light-grey and grey colors correspond to the areas of relatively high (>200 J m^2 K s$^{1/2}$) inertia, while dark-grey colors are for low-inertia areas. The boundaries of persistently wet (white contours) and persistently dry (black contours) spots (compare with Fig. 18) as well as the circles with their areas proportional to the number of MOC images within a given area are superimposed on these maps. Sectors inside the circles indicate the absence (white) or the presence of layered deposits of type 1 (black) and 2 (grey) observed in the images within these areas. The sector sizes are proportional to the number of images within the region, where the layered deposits of type 1 and 2 are seen or where they are not observed.

It is seen in Fig. 20 that the persistently wet spots and the layered deposits of the first type are preferably distributed in the zone of high albedo and low thermal inertia, and that the persistently dry spots and the layered deposits of the second type are preferably distributed in the zone of low albedo and increased thermal inertia. The combination of high albedo and low thermal inertia indicates the presence of a dust blanket. Therefore, the presence of dust on the surface favors the enhanced water abundance. Recall that the above geotraverse analysis has also led to the conclusion that the enhanced water abundance within the Arabia Terra anomaly is somehow related to the presence of dust on the surface.

This analysis also explains the difference between the distinguished types of layered deposits. Most likely, the layered deposits of the first type and the adjacent deposits showing no layering are simply covered with a dust blanket, which makes everything seen bright. A real difference in the brightness of the layered deposits of the first type and their surroundings is not clear from these images. The layered deposits of the second type and their surroundings are probably less dusty, and the material of these layers is actually brighter than their surroundings. Since the layered deposits of both types are very similar in the layering character and in the thickness of layers and since they are quite often developed in the neighborhood, one may suppose that the materials of the layered deposits of the first and second types have the same nature and actual brightness.

It is known that dust plays a key role in condensation of water (ice) from the atmosphere: dust particles serve as condensation nuclei. Moreover, the presence of a layer of deposited dust decreases the surface thermal inertia. This suggests that the enhanced water abundance in the geographically antipodal areas of the equatorial zone might appear due to the retention of moisture from the atmosphere. The moisture could be retained not only by the ice sedimentation, but also by the absorption into porous media and formation of hydrated minerals.

NUMERICAL MODELING OF WATER TRANSPORT BETWEEN THE ATMOSPHERE AND THE SURFACE

To analyze our hypothesis, we numerically simulated the seasonal climatic cycle on Mars with an atmospheric general circulation model. The model was developed by Wilson and his colleagues (Wilson and Hamilton, 1996) and is based on the SKYHI dynamical core developed at the Geophysical Fluid Dynamics Laboratory (Princeton University, USA). Besides the general circulation of the atmosphere, the model includes the description of advection of dust, water vapor, and clouds, the microphysics of condensation clouds, and the self-consistent calculation of the radiative transfer in aerosols. For a thorough description of the model, we refer an interested reader to the papers by Richardson and Wilson (2002) and Richardson et al. (2002). Nevertheless, taking into account the interdisciplinary character of the present study, we think it is necessary to give here the basic information on the model and on the approximations used there.

The primitive equations of meteorology are solved in the hydrostatic approximation on a 3D grid in σ-coordinates. The time integration is performed explicitly using the leapfrog scheme (Roache, 1972) with a time step of 1 to 3 min. Like in other general circulation models of planetary atmospheres of such a class, the temperature field is computed by modeling the solar and thermal radiation transfer and taking into account heat advection by large-scale circulation. In the Martian atmosphere, the radiative transfer is realized by atmospheric gases in the molecular bands and by atmospheric aerosols in the spectral continuum. Only the CO_2 bands are considered among all molecular bands; a high-precision parameterization of Hourdin et al. (1992) is applied. To calculate the radiation field in the spectral continuum, the two-stream approximation is used. The mean effective optical characteristics of the atmosphere are calculated for two wide spectral intervals, corresponding to the solar and thermal IR radiation. Then the radiative transfer equation is solved in each spectral interval with the corresponding boundary conditions, and the obtained fluxes and their divergences are added to the results of the radiative transfer calculations for molecular bands.

The resulting radiative heating rates are taken into account in the energy balance equation in the model's dynamical core, the integration of which yields the temperature field. The surface temperature is calculated based on a simplified 10-layer model of the heat transfer in the regolith due to thermal conduction. The regolith properties in the model are assumed to be constant in depth and characterized by the diffusivity χ, which is specified according to the integral thermal inertia of the

surface. The boundary conditions are built on the basis of the balance of heat fluxes and permit a temperature jump between the surface and the lowest atmospheric model layer. The surface thermal inertia maps obtained from the TES data (Jakosky et al., 2000) and the information on the topography of Mars acquired with the MOLA laser altimeter onboard the *Mars Global Surveyor* spacecraft (Smith et al., 2001) (http://pds-geosciences.wustl.edu/missions/mgs/megdr.html) are used in the model. In addition to the radiation heat exchange, the contribution of the turbulent boundary layer to the thermal flux is taken into account with the usage of the Monin–Obukhov parameterization (Monin and Yaglom, 1992).

An important feature of the model is its capability to self-consistently describe aerosols, including their dust and condensation components, the processes of their transport by atmospheric flows, and the radiative and microphysical processes in aerosols. The size spectrum of dust particles is specified by a set of passive scalar tracers, each of which corresponds to a certain size of dust particles. In its turn, the size spectrum of cloud particles, which are ice crystals, is specified by a set of moments, from zero to third, corresponding to the number density, the mean size, the mean surface area, and the mean volume of particles. The moment method is proved in the papers by Rodin (2002, 2003). Since the dust particles are assumed to be condensation nuclei, the moments of the size distribution of cloud particles associated with the condensation nuclei of a certain size are also described as independent scalar passive tracers in the model. The rates of all microphysical processes related to aerosols—condensation and sublimation, Brownian coagulation, and gravitational sedimentation—as well as their optical properties, are calculated from the set of moments characterizing the size distribution of particles.

The exchange between the atmosphere and the surface is described by the boundary conditions specific for each tracer. The "sticking-wall" boundary conditions are adopted for dust, that is, it is assumed that a dust particle is lost when it reaches the surface. The delivery of dust into the atmosphere is described by specifying the surface sources that parameterize the activity of dust devils. The latter appear when the temperature of the surface exceeds that of the lowest atmospheric layer by more than 22 K. The intensity of these sources and the intensity of dust injection into the atmosphere from the boundary of the polar caps, receding in spring, are the only control parameters of the model. All other processes are described self-consistently. The surface boundary conditions for water vapor and condensation clouds provide the transformation of atmospheric water to precipitation and back depending on the saturation of the lowest atmospheric model layer. The surface reservoir contains precipitated water (frost) and regolith capable to absorb precipitated water. The problems of the model sensitivity to the lower boundary condition for precipitated water were thoroughly studied by Richardson and Wilson (2002).

We adopted a typical scenario corresponding to the present-day climate on Mars and calculated several annual mean integral characteristic that in our opinion can help to understand the nature of the global distribution of the subsurface water storage in the equatorial region. Without going into details of the atmosphere–surface exchange, it is natural to suppose that a sink of water from the atmosphere to the regolith is most effective, when (1) there is a condensate (frost) deposited onto the surface; (2) the water vapor concentration in the lowest atmospheric layer is high; and (3) the soil is colder than the lowest atmospheric layer and can serve as a cold trap.

No doubt, all the above cannot ensure the stability of the subsurface water reservoirs and can only suggest the conditions favoring these reservoirs to be formed or recharged.

Based on the criteria mentioned above, we calculated the annual averages of the following quantities: the exposition of water condensate (frost) on the surface, the water vapor concentration in the lowest atmospheric model layer, and the temperature contrast between the surface and the atmosphere. The distributions of these quantities in the map of Mars are shown in Fig. 21 (a, b, c). While calculating the annual averages, arbitrary thresholds were applied to some parameters. For example, the precipitated water thickness was required to be larger than 100 μm when we calculated the time of the frost existence in a certain surface region (Fig. 21a). No threshold was applied to the water vapor concentration when its annual integral was calculated (Fig. 21b), but the temperature of the lowest atmospheric model layer was required to exceed 220 K. As a measure of the annual mean temperature contrast between the surface and the atmosphere (Fig. 21c), the time was chosen during which this contrast exceeds 30 K and the atmospheric temperature exceeds 200 K. All these quantities serve as illustrations and cannot by themselves help to quantitatively estimate the sink of the atmospheric water to the regolith. To do this, the calculations using the detailed model of the subsurface water reservoirs coupled to the general atmospheric circulation model are needed. This task is beyond the scope of the present paper. The calculations presented here focus on the search of a possible link between the atmospheric processes and the water distribution observed in the Martian regolith rather than on the quantitative explanation of this distribution.

The three maps considered above (Figs. 21a–c) contain the antipodal features in the equatorial region, whose locations approximately correspond to the areas of the low epithermal neutron flux (Fig. 21d). Undoubtedly, there is no exact coincidence, but it is noteworthy that the deviation from the equatorial symmetry and a general contour of the areas of the maximal exposition of frost (Fig. 21a) and water vapor (Fig. 21b) coincide with the analogous deviations and the contour of the areas with enhanced water abundance. As for the tem-
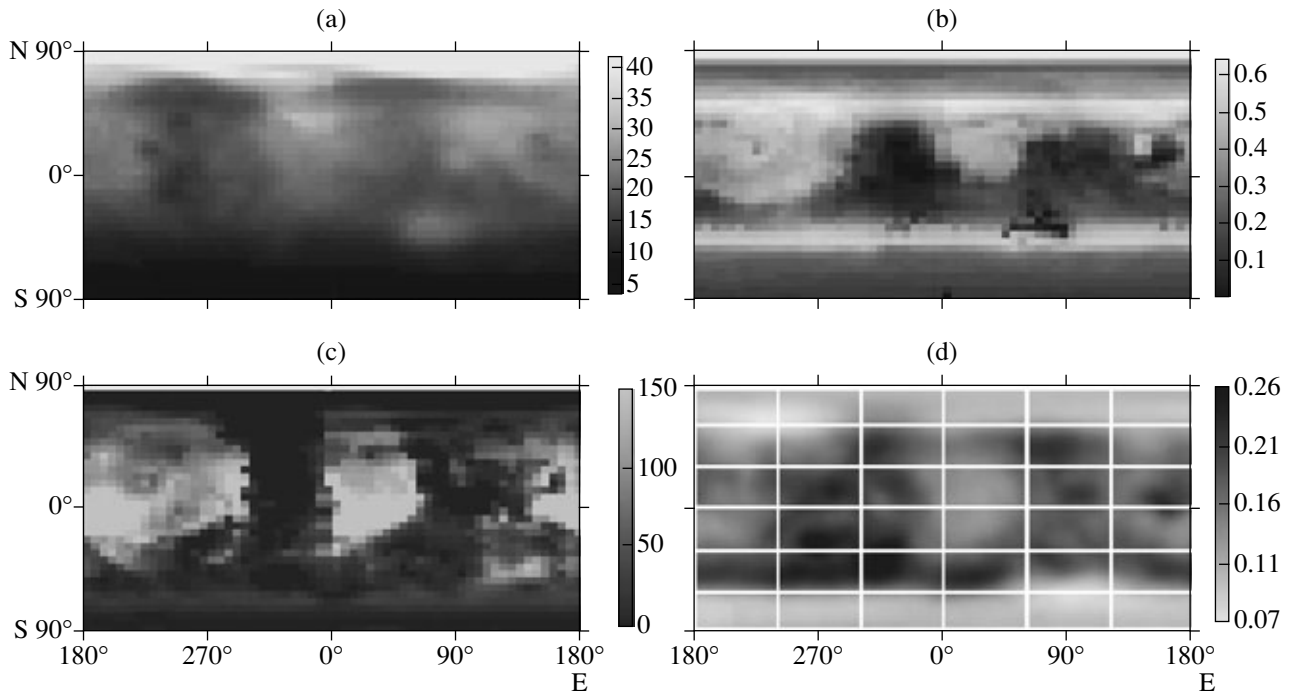
Fig. 21. Maps of (a) the annual exposition (in days) of water condensate (frost) on the surface with a thickness larger than 100 µm, (b) the annual integral of the water vapor content (in cm^{-3}) in the lowest atmospheric model layer at a temperature higher than 220 K, (c) the exposition (in days) of the surface–atmosphere temperature contrast larger than 30 K at a temperature higher than 200 K, and (d) the epithermal neutron flux (count/s) from the HEND data.

perature contrast (Fig. 21c), although the configuration of the areas of maximal contrast differs noticeably, they are at the same longitudes as the features shown in Figs. 21a, b, and d. Since the areas of the maximal temperature contrast are much more extended in the north-to-south direction, one may suppose that the water sink to the regolith is most effective in the places, where other conditions, specifically, a sufficient atmospheric water supply from outside, are provided in addition to the temperature contrast.

Our conclusions also agree with the assumption that the Martian cryosphere rather than the atmosphere was a source of moisture necessary for the formation of the anomalies considered. If there is a weak moisture flux from the Martian interior, the thermodynamic conditions in the anomaly regions block the moisture in the uppermost regolith layer bordering the atmosphere. Since the present-day meteorological conditions in the anomaly regions favor to a moisture sink from the atmosphere and, correspondingly, inhibit the regolith desiccation, and since the flux exhibits diurnal variations of its direction, the difference between the two scenarios can be found only from the knowledge of the direction of the average water fluxes between the cryosphere, atmosphere, and polar caps. However, no data of this kind are available now, and the budget of the Martian hydrological cycle is considered to be stationary within observational errors. Since the amount of water we discuss, if presented as a pure ice, gives a

layer of only a few tens of centimeters, it can be accumulated during tens thousands of years, i.e., during the period characterizing the stable climate state. Consequently, with the current understanding of the climatic processes on Mars, there is no sense in distinguishing an increased sink from the atmosphere and a decreased sink from the regolith: for the same reasons, both scenarios lead to accumulation of the shallow subsurface water resources.

The configuration of areas of the maximal temperature contrast also points to the possible causes of the antipodality of the features under consideration. As well seen from Fig. 21c, they have arcwise contours from the east, which is typical of tidal waves. A simple analysis of model calculations shows that this pattern appears due to the interference of the diurnal cycle of the surface temperature and a tidal daily component with a zonal wave number two. The planetary waves with a zonal number two are reliably detected in the temperature field of the Martian atmosphere (Banfield et al., 2000). Stationary waves with a zonal number two are well seen in the mean annual distributions of water vapor (Smith, 2001), especially during the equinox (Fedorova et al., 2004). It is natural to suppose that the climatic peculiarities of the Arabia Terra region and its antipodal region southwest of Olympus Mons are also caused by the influence of planetary stationary waves. Such waves could provide a preferable sink of dust onto the surface in the areas mentioned, which was followed

by the decrease in the surface thermal inertia and, as a result, the formation of cold traps favoring the water sink from the atmosphere to the uppermost regolith layer in these regions.

Since the pattern of global stationary waves in the atmosphere depends on a large-scale relief of the planet, which has been practically unchangeable from the time of the Tharsis bulge formation (about 3.5 Ga (Neukum and Hiller, 1981; Hartmann and Neukum, 2001)), the location of the regions of the atmospheric moisture sink has probably also been stable over the same long period. At the same time, the general circulation pattern, including the spectrum and the phase structure of the stationary planetary waves, depends on such a time-variable parameter as an inclination of the rotation axis of the planet, as well as on the atmospheric density, which for the past could be different from that of the present time. In numerical experiments with the general circulation model of the Martian atmosphere fulfilled at substantial axis inclinations, Mishna et al. (2003) found that a sink of atmospheric water is maximal in the tropics in the areas of large thermal inertia and high elevation, which contradicts our conclusion. Therefore, according to our hypothesis, the equatorial regions of Mars with enhanced water abundance in the upper regolith layer can be rather young. However, the estimates with a model of age and thickness of the studied anomalies require a thorough analysis of the atmosphere–regolith exchange mechanisms, as well as an extrapolation of the model results to geologically long periods, which is beyond the scope of the present study.

POSSIBLE FORMS OF WATER RETENTION IN THE ANOMALY REGIONS

As has been noted above, hydrogen in the layer where the registered neutron flux originates is likely in the form of water: free (water ice) or bound physically (adsorbed) or chemically (in the structures of minerals as OH and H_2O). Let us consider these cases.

Free Water

Due to stably negative temperatures at the depths of the epithermal neutron flux formation (from 20–30 cm to 1–2 m), it is usually believed that free water, if available, must be in the form of ice there. However, as has been already mentioned, the calculations by Farmer and Doms (1979) and Mellon and Jakosky (1993, 1995) show that water ice must be unstable at these depths. Schorghofer and Aharonson (2005) took into account seasonal variations of air moisture in their model and found that the ice can be stable under some conditions, in particular, at low thermal inertia. In the model by Helbert et al. (2005), subsurface ice is metastable at these depths: it disappears, but slowly in geologic scale.

In general, modeling results of different authors do not agree well so far.

Mangold et al. (2004) showed that, at high latitudes (from 55° to 80° N and S), where the neutron spectrometry points to the presence of a substantial amount of water ice (>8–9 mass % corresponding to 24–27% in volume) in the surface layer, permafrost polygons develop. These polygons result from the fracturing of the icy material of the surface layer due to seasonal and diurnal temperature variations and from the sublimation of the ice outcropping from the fractures. These authors noted that permafrost polygons are not typical of the Arabia Terra and southwest of Olympus Mons anomalies. Our observations also indicate the absence of permafrost polygons within the Arabia Terra anomaly. We saw them only in three images of the geotraverse to the north of the anomaly and in one image at the northern boundary of the anomaly. Inside the anomaly, including the spot at 10° N, 30° E, where according to Mitrofanov et al. (2004) the water abundance reaches 16 mass % (48% in volume, if it is ice), no permafrost polygons are seen. Probably, the presence of water ice is not the cause of the low epithermal neutron flux within Arabia Terra.

Jakosky et al. (2005) supposed that high water contents best agree with the presence of ice in the Martian regolith and analyzed a possible link between the observed distribution of hydrogen (ice) and a number of observed and calculated physical parameters, which can in principle control its distribution in the regolith. From a comparison of the distribution maps for ice and these parameters and from the coefficients of pair and multiple correlation, these authors revealed a link between the ice content and the combination of the mean annual temperature, the geographical latitude, the peak atmospheric water abundance, and the elevation of the place observed. However, this link is weak, and the authors conclude that the accumulation and stable existence of water ice that conform to the observations at low and middle latitudes are impossible under the present conditions.

They seek the solution of the problem in the possible accumulation of a high content of ice over past geologic epochs and in its partial preservation now. The higher content of ice can be accumulated in the regolith at higher atmospheric water contents. The latter must have been at a higher inclination of the rotation axis of the planet to the orbit plane, when the polar caps are heated to high temperatures in summer seasons. The last time such a situation might have occurred was $\sim 10^5$ years ago (see, e.g. Jakosky et al., 1995; Laskar et al., 2002; Mishna et al., 2003). However, this requires the accumulated ice to have survived at a depth of less than a meter for 10^5 years, which seems to be of low probability.

Jakosky et al. (2005) see another possibility of the appearance of higher water contents in the atmosphere. They point out that, according to the model by Jakosky
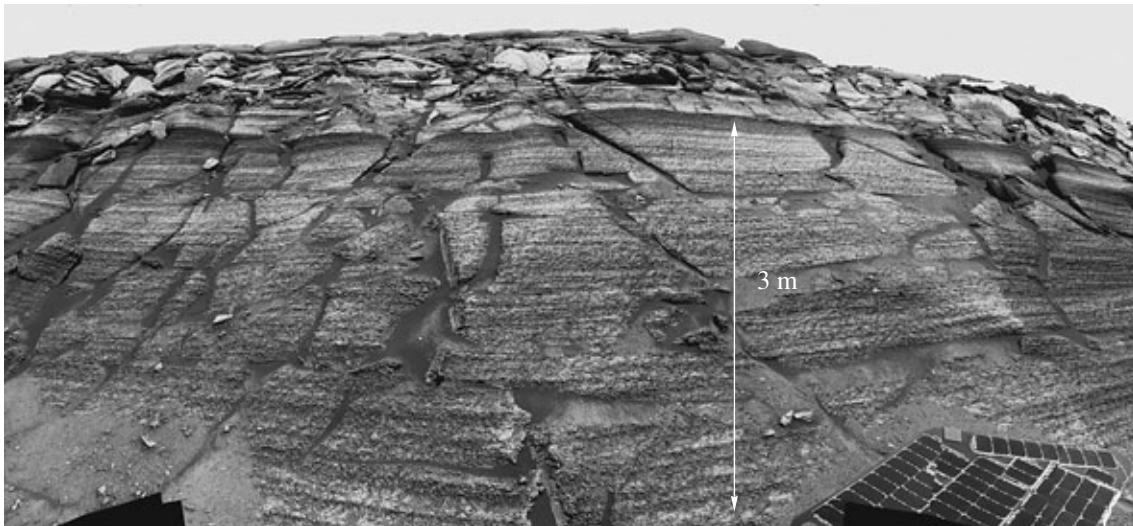
Fig. 22. Outcrops of fine-layered rocks with a high content of hydrated magnesium sulfates in the Endurance Crater, a landing site of the *Opportunity* rover. The fragment of the PAI07110 image (the JPL NASA photo-atlas).

and Haberle (1990), two stable regimes of the south polar cap are possible at present conditions. In one regime, which is now the case, the south cap is covered with CO_2 ice in summer. Since this ice prevents the underlying H_2O ice from heating and sublimation, there is not much water in the atmosphere. In the other regime, the CO_2 ice completely disappears from the south cap by about mid-summer, the H_2O ice begins to sublimate, and the mean annual abundance of the atmospheric water may reach 100 precipitated μm. In the authors' opinion, the latter could have been the case as recently as a thousand years ago or even a few decades ago, which makes the preservation of ice possible today. Jakosky et al. (2005) note that, even within the frames of such a model, there is only a partial agreement with the ice distribution observed at low and middle latitudes and consider this as a result of the model imperfection. They also note that the observed distribution shows a zonal wave-number two behavior, which leads to our model suggested in the previous section.

At negative temperatures, free water may also exist in the form of brines (see, e.g., Brass, 1980; Kuzmin and Zabalueva, 1998). Brines with a high content of $CaCl_2$ remain liquid up to 220–225 K. However, it is evident that they must evaporate in the case of a long contact with the atmosphere. For a short time, the brines may appear on the Martian surface or nearby. It is probable that the soil brines are responsible for the seasonal increase in the radar reflectivity observed in several regions of Mars (see, e.g., Zisk and Mouginis-Mark, 1980; Roth et al., 2002). However, the Arabia Terra anomaly and its antipode are the phenomena observed throughout a year, and no radar anomaly has been noticed there. It is clear that brines do not cause a low epithermal neutron flux within Arabia Terra.

Adsorbed Water

As has been mentioned above, laboratory experiments by Zent and Quinn (1995) show that the abundance of adsorbed water under the Martian surface conditions unlikely exceeds 0.1–0.2 mass % even in the highly-porous material like palagonite. The same conclusion was obtained by these authors in the study of water adsorption by the clay mineral Na smectite (Zent, 1995; Zent et al., 2001). Jakosky et al. (2005) concluded the same. On the contrary, some other data suggest the possibility of high abundances of absorbed water. For example, Bish et al. (2003) reduced the experimental data on the water adsorption by Ca smectite and some zeolites obtained under indoor temperature to the Martian surface conditions and concluded that the adsorption of water by these minerals can be responsible for a high abundance of hydrogen in the discussed anomalies of the Martian equatorial region. Thus, the question on the role of adsorption remains open.

Chemically Bound Water

Basilevsky et al. (2003) concluded that the decrease in the epithermal neutron flux in Arabia Terra and southwest of Olympus Mons is likely caused by the enhanced concentration of materials containing chemically bound water (clay minerals, palagonite, hydroxides, and hydrosalts) in the surface layer of these regions. New data on this problem have appeared since 2003. First of all, these are the results obtained with the instruments onboard the *Opportunity* rover, which landed in the southwestern part of the Arabia Terra anomaly (Squyres et al., 2004a, 2004b).

There are outcroppings of relatively bright (with albedo of 0.25 ± 0.06) layered rocks on the inner slopes

of impact craters (Fig. 22) at the landing site and in its vicinity (Bell et al., 2004). These rocks contain a mixture of relatively rounded small silicate (olivine and pyroxene) debris grains, hematite oolites 4–6 mm in diameter, and fine-grained cement mainly composed of Mg and Ca sulfates. On average, the content of the silicate component, hematite, and sulfate minerals is ~50 mass %, ~10%, and ~40% respectively (Squyres et al., 2004a). In the MOC images, the layered rocks are seen not only at the landing site, but also on a large area around: at least on tens thousands squared kilometers (Squyres et al., 2004a). In fact, this is a region of the hematite-containing deposits in Sinus Meridiani found from the TES data (Christensen et al., 2001b). There are probably also a lot of sulfates in the Arabia Terra layered deposits observed in the MOC images outside the hematite zone. Recall that a part or, probably, the main part of the layered rocks considered above in the description of persistently wet and persistently dry spots of the Arabia Terra anomaly are also relatively bright.

Fialips et al. (2005) consider a possible link between the hydrogen (water) distribution observed at low and middle latitudes with the presence of some clays, zeolite, and hydrated magnesium sulfates in the regolith. A thermodynamic analysis shows that these minerals are thermodynamically stable in the Martian regolith, which agrees with the data of other studies (see, e.g., Shapkin and Sidorov, 2004; Zolotov, 1988). However, in order to provide the observed high abundance of hydrogen, the content of clay minerals and zeolite in the regolith must be unlikely high (50–70%), while the required contents of magnesium sulfates seem to be realistic (2–11%) in the case of epsomite and hexahydrite (Fialips et al., 2005). Thus, if the high hydrogen abundance observed at low and middle latitudes is attributed to the chemically bound water, its carrying minerals are most likely hydrated magnesium sulfates.

In our model, explaining the antipodal anomalies by a sink of water vapor from the atmosphere in several distinctive regions of the planet, these anomalies are geologically young. This poses the question on the retaining kinetics of bound water in the Martian regolith under present-day conditions: "Is such retention fast enough?" The answer to this question is provided by the analysis of the results on the IR mapping of the Martian surface through a Martian year with the TES instrument (Kuzmin et al., 2005). The authors use the bound-water index (BWI) suggested in their earlier work (Kuzmin et al., 2004). This index is based on the measurements of the radiation intensity at a bound-water frequency (1640 cm^{-1}) and at several neighboring frequencies. Although Kuzmin et al. (2005) do not discuss the problem of the water-distribution antipodal anomalies, their BWI maps clearly show seasonal variations of this index within the anomalies under consideration. This means that seasonal changes are accompanied by the binding of water into minerals and the inverse processes on the surface of anomalous zones

(and not only there), which clearly indicates the absence of kinetic constraints on the chemical binding of water coming from the atmosphere. Interestingly, the results of the experiments on the hydration–dehydration kinetics of magnesium sulfates show that these processes are rather quick (days, months) (Chipera et al., 2005; Vaniman et al., 2005). This benefits the above supposition that the water responsible for the neutron flux anomalies is bound in hydrated magnesium sulfates.

DISCUSSION

In the present paper, we have attempted to find the geological causes of the anomalously low neutron flux observed in the Arabia Terra region. For this purpose, we examined 152 narrow-angle MOC images and the context wide-angle images within the geotraverse crossing the anomaly. While examining the images, we paid attention to the presence of layered deposits, fluvial valleys, polygons, debris flows, dunes, dust devil traces, and to the prevailing type of the surface texture. From the morphology of small impact craters, we estimated the minimal thickness of loose surface mantle in a given place. For the most part of these features, we found no preferable link with the anomaly. The correlation was revealed only for dust devil traces: they were observed only inside the anomaly. There is probably also a link with a prevailing surface texture type: the smooth and fine-texturized surfaces dominate within the anomaly. The connection with dust devil traces and predominance of smooth and fine-texturized surfaces is indicative of the enhanced dustiness of the anomalous region.

For the "core" of the Arabia Terra anomaly, the sigma parameter (see above) was mapped, which allowed the "persistently wet" and "persistently dry" spots to be distinguished; and all the 122 narrow-angle MOC images within these spots were examined. It was found that the persistently wet spots preferably reside in the areas of high albedo and low surface thermal inertia, while the persistently dry spots are in the areas of relatively low albedo and the higher thermal inertia. Since on Mars the combination of high albedo and low thermal inertia indicates the dust abundance, this preference leads to some connection between the moisture detected by neutron spectrometers and the presence of dust.

Since dust plays an important role in condensation of water from the atmosphere, we supposed that the enhanced water content in the regolith of Arabia Terra and its geographically antipodal region appeared probably due to the moisture retention from the atmosphere. To analyze this assumption, we numerically simulated the seasonal climatic cycle of Mars using the atmospheric general circulation model. From this modeling, the parameters responsible, in our view, for a sink of atmospheric moisture to the regolith were mapped. These parameters are: the exposition of condensed

water (frost) on the surface, the concentration of water vapor in the lowest atmospheric model layer, and the temperature contrast between the surface and the atmosphere. It has turned out that the distribution of these meteorological parameters throughout the planet agrees rather well (especially, for the first two parameters) with the geographical location of the observed anomalies. As has been mentioned above, we cannot exclude that the Martian cryosphere, not the atmosphere, was a source of moisture for the formation of the studied anomalies. If there is a weak moisture flux from the Martian interior, the thermodynamic conditions in the anomaly regions can lock it in the uppermost regolith layer at the boundary with the atmosphere.

As has been already mentioned, under the present Martian surface conditions, ice is likely unstable at the latitudes of the anomalies at the depths accessible to neutron-spectrometric remote sensing. Jakosky et al. (2005) believe that the anomalies can be caused by relic ice deposits that have survived from a recent (according to their model) time when the ices' sublimation regime was different from the current one: CO_2 ice sublimated completely in the first half of summer and H_2O ice sublimated intensively in the second half of summer. We do not deny such a possibility, but suppose that the coincidence of the geographical location of the zones presently favorable for a water sink from the atmosphere with the position of the anomalies under consideration more likely evidences the recent character of the processes of water accumulation inducing the neutron flux anomaly.

Feldman et al. (2005) also hold to the idea that the anomalies under consideration were formed recently. By the example of six meridional profiles, they found the correlation between the relative maximums of water content at low and middle latitudes and the relative maximums of the surface elevation. From this, they infer that this is a result of the water vapor diffusion, controlled by weather conditions, into the regolith.

Since ice is unstable at the sounded depths, the moisture delivered from the atmosphere is probably chemically bound, and hydrated magnesium sulfates seem to be the best candidate for the carrier phase inducing the water anomaly. The results of the experiments on the hydration–dehydration kinetics of magnesium sulfates (Chipera et al., 2005; Vaniman et al., 2005) and observations of the seasonal variations of the bound-water index on the Martian surface (Kuzmin et al., 2005) do not contradict this supposition.

CONCLUSIONS

From all the above, we conclude that the antipodal anomalies observed with the neutron spectrometers and indicating the enhanced hydrogen content in the upper 1–2 m of the regolith of the anomalous region are more likely recent rather than ancient formations. Probably,

they were formed by the moisture sink from the atmosphere in the places where such a sink is favored by the present meteorological conditions. The geological parameters controlling these conditions, first of all, the presence of dust on the surface, are probably also connected to meteorological processes, especially to atmospheric dust transport and dust sedimentation in the anomaly regions under the action of the planetary wave with a zonal wavenumber two. This wavenumber determines the antipodal character of the anomalies. The intensity of moisture sink depends on the presence of dust in a complex way. The dust particles, which serve as condensation nuclei, maintain the formation of near-surface fogs and the precipitation of condensate onto the surface in the form of frost. However, the main effect of dust is likely connected with the effective thermal insulation of the regolith, which leads to decreased thermal inertia. The surface, whose thermal inertia is low, quickly cools at night to form a cold trap for atmospheric moisture. It is not improbable that the Martian cryosphere rather than the atmosphere is a source of moisture for the formation process of the anomalies studied: the thermodynamic conditions in the anomaly regions may lock the moisture flux from the Martian interior in the uppermost regolith layer. The moisture coming from the atmosphere or from the interior is probably retained as chemically bound water entering the structure of water-bearing minerals (likely, hydrated magnesium sulfates) directly from the vapor; or the moisture precipitated as frost penetrates into microfissures and then is bound in minerals. Probably, another geologic factor can work in the Arabia Terra anomaly, namely, the abundance of magnesium sulfates in this area.

ACKNOWLEDGMENTS

REFERENCES

Banfield, D.B., Conrath, J.C., Pearl, M., et al., Thermal Tides and Stationary Waves on Mars as Revealed by Mars Surveyor Thermal Emission Spectrometer, *J. Geophys. Res., Ser. E*, 2000, vol. 105, no. 4, pp. 9521–9538.

Basilevsky, A.T., Ivanov, B.A., Florenskii, K.P., et al., *Udarnye kratery na Lune i planetakh* (Impact Craters on the Moon and Planets), Moscow: Nauka, 1983.

Basilevsky, A.T., Litvak, M.L., Mitrofanov, I.G., et al., Search for Traces of Chemically Bound Water in the Martian Surface Layer Based on HEND Measurements onboard the 2001 *Mars Odyssey* Spacecraft, *Astron. Vestn.*, 2003, vol. 37, no. 5, pp. 423–434 [*Sol. Syst. Res.* (Engl. Transl.), vol. 37, no. 5, pp. 387–396].

Bell, J.F.., Squyres, S.W., Arvidson, R.E., et al., Pancam Multispectral Imaging Results from the *Opportunity* Rover at Meridiani Planum, *Science,* 2004, vol. 306, pp. 1703–1709.

Biemann, K., Oro, J., Toulmin, P., III, et al., The Search for Organic Substances and Inorgainic Volatile Compounds in the Surface of Mars, *J. Geophys. Res.*, 1977, vol. 82, pp. 4641–4658.

Bish, D.L., Carey, J.W., Vaniman, DT., and Chipera, S.J., Stability of Hydrous Minerals on the Martian Surface, *Icarus,* 2003, vol. 164, pp. 96–103.

Boynton, W.V., Feldman, W.C., Squyres, S.W., et al., Distribution of Hydrogen in the Near Surface of Mars: Evidence for Subsurface Ice Deposits, *Science,* 2002, vol. 297, pp. 81–85.

Brass, G.W., Stability of Brines on Mars, *Icarus,* 1980, vol. 42, pp. 20–28.

Carr, M., *Water on Mars*, New York: Oxford Univ. Press, 1996.

Chipera, S.J., Vaniman, D.T., Bish, D.L., et al., Experimental Stability and Transformation Kinetics of Magnesium Sulfate Hydrates that May Be Present on Mars, *Lunar Planet. Sci.*, 2005, vol. 36, Abstract #1497.

Christensen, P.R., Bandfield, J.L., Hamilton, V.C., et al., Mars Global Surveyor Thermal Emission Spectrometer Experiment: Investigation Description and Surface Science Results, *J. Geophys. Res.*, 2001, vol. 106, pp. 23873–23885.

Christensen, P.R., Malin, M.C., Morris, R.V., et al., Martian Hematite Mineral Deposits: Remnants of Water Driven Processes on Early Mars, *J. Geophys. Res.*, 2001, vol. 106, p. 885.

Edgett, K.S., Butler, B.J., Zimbelman, J.R., and Hamilton, V.E., Geologic Context of the Mars Radar "Stealth" Region in Southwestern Tharsis, *J. Geophys. Res.*, 1997, vol. 102, p. 567.

Farmer, C.B. and Doms, P.E., Global and Seasonal Water Vapor on Mars and Implications for Permafrost, *J. Geophys. Res.*, 1979, vol. 84, pp. 2881–2888.

Fedorova, A.A., Rodin, A.V., and Baklanova, I.V., MAWD Observations Revisited: Seasonal Behavior of Water Vapor in the Martian Atmosphere, *Icarus,* 2004, vol. 171, pp. 54–67.

Feldman, W.C., Boynton, W.V., Tokar, R.L., et al., Global Distribution of Neutrons from Mars: Results from *Mars Odyssey, Science,* 2002, vol. 297, pp. 75–78.

Feldman, W.C., Prettyman, T.H., Maurice, S., et al., Topographic Control of Hydrogen Deposits at Low Latitudes of Mars, *J. Geophys. Res., Ser. E*, 2005, vol. 110, p. 11009.

Ferri, F., Smith, P.H., Lemmon, M., and Renno, N.O., Dust Devils As Observed by *Mars Pathfinder, J. Geophys. Res., Ser. E*, 2003, vol. 108, no. 12, Cite 5133.

Fialips, C.I., Carey, J.W., Vaniman, D.T., et al., Hydration States of Zeolites, Clays, and Hydrated Salts Under Present-Day Martian Surface Conditions: Can Hydrous Minerals Account for Mars Odyssey Observations of Near Equatorial Water-Equivalent Hydrogen, *Icarus,* 2005, vol. 178, no. 1, pp. 74–83.

Greeley, R. and Guest, J.E., Geologic Map of the Eastern Equatorial Region of Mars, *Atlas of Mars*, Map I-1802-B, USGS, 1987.

Hartmann, W.K. and Neukum, G., Cratering Chronology and Evolution of Mars, *Space Sci. Rev.*, 2001, vol. 96, pp. 165–194.

Helbert, J., Reiss, D., Hauber, E., and Benkhoff, J., Limits on the Burial Depth of Glacial Ice Deposits on the Flanks of Hecates Tholus, Mars, *Geophys. Rev. Lett.*, 2005, vol. 32, Cite ID.L17201.

Hourdin, F., A New Representation of the Absorption by the CO_2 15-Microns Band for a Martian General Circulation Model, *J. Geophys. Res., Ser. E*, 1992, vol. 97, no. 11, pp. 18319–18335.

Howard, A.D., Moore, J.M., and Irwin, R.P., An Intense Terminal Epoch of Widespread Fluvial Activity on Early Mars: 1. Valley Network Incision and Associated Deposits, *J. Geophys. Res., Ser. E*, 2005, vol. 110, no. 12, p. 14.

Irwin, R.P., Howard, A.D., Craddock, R.A., and Moore, J.M., An Intense Terminal Epoch of Widespread Fluvial Activity on Early Mars: 2. Increased Runoff and Paleolake Development, *J. Geophys. Res., Ser. E*, 2005, vol. 110, no. 12, p. 15.

Jakosky, B.M. and Haberle, R.M., Year-To-Year Instability of the Mars South Polar Cap, *J. Geophys. Res.*, 1990, vol. 95, pp. 1359–1365.

Jakosky, B.M., Henderson, B.G., and Mellon, M.T., Chaotic Obliquity and the Nature of the Martian Climate, *J. Geophys. Res.*, 1995, vol. 100, pp. 1579–1584.

Jakosky, B.M., Mellon, M.T., Kieffer, H.H., et al., The Thermal Inertia of Mars from the Mars Global Surveyor Thermal Emission Spectrometer, *J. Geophys. Res.*, 2000, vol. 105, pp. 9643–9652.

Jakosky, B.M., Mellon, M.T., Varnes, E.S., et al., Mars Low-Latitude Neutron Distribution: Possible Remnant Near-Surface Water Ice and a Mechanism for Its Recent Emplacement, *Icarus,* 2005, vol. 175, no. 1, pp. 58–67.

Kozyrev, A.S., Mitrofanov, I.G., Litvak, M.L., et al., Subsurface Water Distribution in Martian Equatorial Regions from HEND/Odyssey Data, *Vernadsky-Brown Microsymposium 38*, Moscow, 2003, Abstract MS050 (CD-ROM).

Kuzmin, R.O. and Zabalueva, E.V., On Salt Solutions in the Martian Cryolithosphere, *Astron. Vestn.,* 1998, vol. 32, no. 3, pp. 213–225 [*Sol. Syst. Res.* (Engl. Transl.), vol. 32, no. 3, pp. 187–197].

Kuzmin, R.O., Christensen, P.R., and Zolotov, M.Yu., Global Mapping of Martian Bound Water at 6.1 Microns Based on TES Data: Seasonal Hydration-Dehydration of Surface Minerals, *Lunar Planet. Sci.*, 2004, vol. 35, Abstract #1810.

Kuzmin, R.O., Christensen, P.R., Zolotov, M.Yu., and Anwar, S., Seasonal Variations of the Bound Water Content on the Martian Surface: Global Mapping of the 6.1 μm Emissivity Band Based on TES Data, *Vernadsky-Brown Microsymposium 42*, Moscow, 2005, Abstract ms42-42 (CD-ROM).

Lane, M.D., Christensen, P.R., and Hartmann, W.K., Utilization of the THEMIS Visible and Infrared Imaging Data for Crater Population Studies of the Meridiani Planum Landing Site, *Geophys. Rev. Lett.*, 2003, vol. 30; DOI: 10.1029/2003GL017183.

Laskar, J., Levrard, B., and Mustard, J.F., Orbital Forcing of the Martian Polar Layered Deposits, *Nature,* 2002, vol. 419, pp. 375–377.

Malin, M.C. and Edgett, K.S., Sedimentary rocks of early Mars, *Science,* 2000, vol. 290, no. 5498, pp. 1927–1937.

Malin, M.C. and Edgett, K.S., *Mars Global Surveyor* Mars Orbiter Camera: Interplanetary Cruise Through Planetary Mission, *J. Geophys. Res.,* 2001, vol. 106, pp. 23409–23570.

Mangold, N., Maurice, S., Feldman, W.C., et al., Spatial Relationships Between Patterned Ground and Ground Ice Detected by the Neutron Spectrometer on Mars, *J. Geophys. Res., Ser. E,* 2004, vol. 109, p. 08001.

Mellon, M.T. and Jakosky, B.M., Geographic Variations in the Thermal and Diffusive Stability of Ground Ice on Mars, *J. Geophys. Res.,* 1993, vol. 98, pp. 3345–3364.

Mellon, M.T. and Jakosky, B.M., The Distribution and Behavior of Martian Ground Ice During Past and Present Epochs, *J. Geophys. Res.,* 1995, vol. 100, pp. 11781–11800.

Mellon, M.T., Jakosky, B.M., Kieffer, H.H., and Christensen, P.R., High Resolution Thermal-Inertia Mapping from the Mars Global Surveyor Thermal Emission Spectrometer, *Icarus,* 2000, vol. 148, pp. 437–455.

Mishna, M.A., Richardson, M.I., Wilson, R.J., and McCleese, D., On the Orbital Forcing of Martian Water and CO_2 Cycles: A General Circulation Model Study with Simplified Volatile Schemes, *J. Geophys. Res.,* 2003, vol. 108, p. 16-1, Cite ID 5062; DOI: 10.1029/2003JE002051.

Mitrofanov, I., Anfimov, D., Kozyrev, A., et al., Maps of Subsurface Hydrogen from High Energy Neutron Detector, *Science,* 2002, vol. 297, pp. 78–81.

Mitrofanov, I.G., Litvak, M.L., Kozyrev, A.S., et al., Search for Water in Martian Soil Using Global Neutron Mapping by the Russian HEND Instrument Onboard the US 2001 *Mars Odyssey* Spacecraft, *Astron. Vestn.,* 2003, vol. 37, no. 5, pp. 400–412 [*Sol. Syst. Res.* (Engl. Transl.), vol. 37, no. 5, pp. 366–377].

Mitrofanov, I.G., Litvak, M.L., Kozyrev, A.S., et al., Soil Water Content on Mars as Estimated from Neutron Measurements by the HEND Instrument Onboard the 2001 *Mars Odyssey* Spacecraft, *Astron. Vestn.,* 2004, vol. 38, no. 4, pp. 291–303 [*Sol. Syst. Res.* (Engl. Transl.), vol. 38, no. 4, pp. 253–265].

Monin, A.S. and Yaglom, A.M., *Statisticheskaya gidromekhanika. Teoriya turbulentnosti* (Statistical Fluid Mechanics. Theory of Turbulence), St. Petersburg: Gidrometeoizdat, 1992.

Neukum, G. and Hiller, K., Martian Ages, *J. Geophys. Res.,* 1981, vol. 83, pp. 5455–5464.

Newsom, H.E., Barber, C.A., Hare, T.M., et al., Paleolakes and Impact Basins in Southern Arabia, Including Meridiani Planum: Implications for the Formation of Hematite Deposits on Mars, *J. Geophys. Res., Ser. E,* 2003, vol. 108, no. 12, p. 8075; DOI: 10.1029/2002JE001993.

Pike, R.J. and Davis, P.A., Towards a Topographic Model of Martian Craters from Photoclinometry, *Lunar Planet. Sci.,* 1984, vol. 15, pp. 645–646.

Renno, N.O., Nash, A.A., Lunine, J., and Murphy, J., Martian and Terrestrial Dust Devils: Test of a Scaling Theory Using Pathfinder Data, *J. Geophys. Res.,* 2000, vol. 105, pp. 1859–1866.

Richardson, M.I. and Wilson, R.J., Investigation of the Nature and Stability of the Martian Seasonal Water Cycle with a General Circulation Model, *J. Geophys. Res., Ser. E,* 2002, vol. 107, no. 5, p. 7-1, Cite ID 5031; DOI: 10.1029/2001JE001536.

Richardson, M.I., Wilson, R.J., and Rodin, A.V., Water Ice Clouds in the Martian Atmosphere: General Circulaton Model Experiments with a Simple Cloud Scheme, *J. Geophys. Res., Ser. E,* 2002, vol. 107, no. 9; DOI: 10.1029/2001JE001804.

Roache, P., *Computational Fluid Dynamics*, Albuquerque: Hermosa, 1972. Translated under the title *Vychislitel'naya gidrodinamika,* Moscow: Mir, 1980.

Rodin, A.V., On the Moment Method for the Modeling of Cloud Microphysics in Rarefied Turbulent Atmospheres: I. Condensation and Mixing, *Astron. Vestn.,* 2002, vol. 36, no. 2, pp. 97–106 [*Sol. Syst. Res.* (Engl. Transl.), vol. 36, no. 2, pp. 97–106].

Rodin, A.V., On the Moment Method for the Modeling of Cloud Microphysics in Rarefied Turbulent Atmospheres: II. Stochastic Coagulation, *Astron. Vestn.,* 2003, vol. 37, no. 2, pp. 101–111 [*Sol. Syst. Res.* (Engl. Transl.), vol. 37, no. 2, pp. 101–111].

Roth, L.E., Saunders, R.S., and Schubert, G., Mars: Seasonally Variable Radar Reflectivity, *Lunar Planet. Sci.,* 2002, vol. 16, pp. 712–713.

Schorghofer, N. and Aharonson, O., Stability and Exchange of Subsurface Ice on Mars, *J. Geophys. Res., Ser. E,* 2005, vol. 110, Cite ID 05003.

Schultz, P.H. and Lutz, A.B., Polar Wandering on Mars, *Icarus,* 1988, vol. 73, pp. 91–141.

Scott, D.H. and Carr, M.H., Geologic Map of Mars, *Atlas of Mars*, Map I-1083, USGS, 1978.

Scott, D.H. and Tanaka, K.L., Geologic Map of the Western Equatorial Region of Mars, *Atlas of Mars*, Map I-1802-A, USGS, 1986.

Shapkin, A.I. and Sidorov, Yu.I., *Termodinamicheskie modeli v kosmokhimii i planetologii* (Thermodynamical Models in Cosmochemistry and Planetology), Moscow: Editorial URSS, 2004.

Smith, D.E., Zuber, M.T., Frey, H.V., et al., *Mars Orbiter* Laser Altimeter: Experiment Summary After the First Year of Global Mapping of Mars, *J. Geophys. Res.,* 2001, vol. 106, pp. 23689–23722.

Smith, M.D., The Annual Cycle of Water Vapor on Mars As Observed by the Thermal Emission Spectrometer, *J. Geophys. Res., Ser. E,* 2001, vol. 107, no. 11, p. 25-1, Cite ID 5115; DOI: 10.1029/2001JE001522.

Squyres, S.W., Arvidson, R.E., and Bell, J.F., III, et al., The Opportunity Rover Athena Science Investigation at Meridiani Planum, Mars, *Science,* 2004a, vol. 306, pp. 1698–1703.

Squyres, S.W., Grotzinger, J.P., and Aridson, R.E., et al. In Situ Evidence for An Ancient Aqueous Environment at

Meridiani Planum, Mars, *Science,* 2004b, vol. 306, pp. 1709–1714.

Vaniman, D.T., Chipera, S.J., Bish, D.L., et al., Martian Relevance of Dehydration and Rehydration in the Mg-Sulfate System, *Lunar Planet. Sci.*, 2005, vol. 36, Abstract #1486.

Wilson, R.J. and Hamilton, K.P., Comprehensive Model Simulation of Thermal Tides in the Martian Atmosphere, *J. Atmos. Sci.*, 1996, vol. 53, pp. 1290–1326.

Zent, A.P. and Quinn, R.C., Simultaneous Adsorption of CO_2 and H_2O Under Mars-Like Conditions and Application To the Evolution of the Martian Climate, *J. Geophys. Res.*, 1995, vol. 100, pp. 5341–5349.

Zent, A.P., Howard, D.J., and Quinn, R.C., H_2O Adsorption on Smectites: Application to the Diurnal variation of H_2O in the Martian Atmosphere, *J. Geophys. Res.*, 2001, vol. 106, p. 14667–14674.

Zisk, S.H. and Mouginis-Mark, P.J., Anomalous Region on Mars: Implications for Near-Surface Liquid Water, *Nature,* 1980, vol. 44, pp. 735–738.

Zolotov, M.Yu., Water-Bearing Minerals in the Martian Soil (Thermodynamic Prediction of Stability), *Lunar Planet. Sci.*, 1988, vol. 20, pp. 1257–1258.